JOURNAL OF APPLIED PHYSICS **109**, 074113 (2011)

# Polyethylene nanocomposite dielectrics: Implications of nanofiller orientation on high field properties and energy storage

V. Tomer,[1,3] G. Polizos,[2] C. A. Randall,[1,a)] and E. Manias[2,b)]
[1]*Center of Dielectric Studies (CDS), Materials Research Laboratory, The Pennsylvania State University, 260 MRL–University Park, Pennsylvania 16802, USA*
[2]*Polymer Nanostructrures Lab–Center for the Study of Polymeric Systems (CSPS), Department of Materials Science and Engineering, The Pennsylvania State University, University Park, Pennsylvania 16802, USA*
[3]*The Dow Chemical Co., Corporate Research & Development, Midland, Michigan 48674, USA*

(Received 8 January 2011; accepted 19 February 2011; published online 15 April 2011)

Nanocomposite formation, through the incorporation of high aspect ratio nanoparticles, has been proven to enhance the dielectric properties of thermoplastic polymers, when the mitigation of internal charges and the nature of the interfacial regions are properly adjusted. Here, we explore polyethylene/montmorillonite nanocomposites, and we specifically investigate how to impart desirable dielectric behavior through controlled nanoscale texturing, i.e., through control of the spatial arrangement of the high aspect ratio nanofiller platelets. In particular, it is shown that filler alignment can be used to improve the high electric-field breakdown strength and the recoverable energy density. The origins of the improved high field performance were traced to improved charge-trapping by a synergy of nanofillers and polar maleic anhydride (MAH) groups—introduced via polyethylene-MAH copolymers—as templated by the inorganic nanofillers. Further, it is conclusively demonstrated that the alignment of the two-dimensional nanoparticles has a measurable positive effect on the breakdown strength of the materials and, consequently, on the maximum recoverable energy density. © *2011 American Institute of Physics*. [doi:10.1063/1.3569696]

## I. INTRODUCTION

Advancements in consumer electronics, pulsed power applications, and hybrid vehicles have necessitated the demand for compact, robust, and transient energy storage systems.[1] Since electrostatic energy storage relates to the permittivity and breakdown field exhibited by a material, it becomes crucial that high-performance dielectrics must possess high dielectric permittivity and, simultaneously, demonstrate high operational electric fields with low dissipation factors.[2–7] Recent developments in polymer composites with nanosized fillers have shown significant improvements in dielectric strength as well as order of magnitude improvements in voltage endurance.[3,4,8–15] These improvements are interesting both in terms of commercial application and for future advancements in nanodielectrics. Furthermore, fundamental insight can also be gained by studying the mechanisms controlling the enhanced dielectric response. Nanocomposites, in certain aspects, can offer much better properties when compared to micro-filled polymer composites. The advantages of the former stemming from low filler loadings, nanometer sizes, and large surface areas.[16,17] The low nanofiller loadings allow for composite formation without altering some of the intrinsic polymeric properties, e.g., density. Nanometer sizes also permit small particle-to-particle distances that can significantly affect the charge transport properties at high operational fields.[15,18,19] Finally, the presence of a large interfacial area facilitates a greater interaction of polymer matrices with fillers and, when properly designed,[3,4] this greater extent of interactions can enhance the dielectric properties of the composite material. All these features offer new opportunities for designing an entirely different class of dielectrics, that could offer higher energy storage or lower dielectric loss, and improved power dissipation.

Thermoplastic polyolefins, such as polyethylene (PE), is traditionally one of the most widely used polymer classes with applications in structural, textile, and packaging industries, and their nanocomposites have found multiple applications for the same uses, when improved performance can be achieved, e.g., flame retardant behavior, or packaging films with low gas permeability and tunable thermomechanical properties.[20–22] More recently, PE nanocomposites have also found various uses in the electrical power industry, in particular, for cable insulation, where conducting properties of carbon black were exploited in cable insulation for field grading, whereas addition of low permittivity nanofiller silica has been shown to improve dielectric breakdown.[10,11] Such behaviors have also instigated an interest in the energy storage capabilities of PE (nano)composites.

The use of nanofillers is shown to be beneficial in stopping partial discharge degradation, increasing voltage endurance, and improving space-charge formation. In contrast, incorporation of microfillers has been suggested to be detrimental to the final properties of the composites. It is believed[11] that nanoadditives in thermoplastics can allow localized charge movement, thereby minimizing bulk charge accumulation and, thus, decrease the likelihood of free electron cascade that ultimately results in disruptive breakdown of polymers. For example, the charge transport process has been argued to be dependent on shallow trap assisted hops in the direction of applied field.[23,24]

---

[a)] Electronic mail: car4@psu.edu.
[b)] Electronic mail: manias@psu.edu.

However, Dissado and Fothergill argue that interstate tunneling is more plausible considering barriers are too high in polymers;[25,26] so it is the scattering processes, rather than trap distributions, that ultimately limit the electron mobilities (although the traps may nonetheless serve as scattering centers). Furthermore, morphological considerations emphasize the postulation that, at a macroscopic level, electronic and mechanical performances may not be distinct:[24] i.e., improved mechanical properties—obtained with better filler dispersion and improved polymer/filler interfaces—could lead to enhanced electrical performance. In the simplest case, mechanical stresses at high fields can lead to structure expansion, increasing the free volume level and generating microvoids that can act as charge traps, which in turn alter the field distribution, thus completing a circle of electrical-mechanical-electrical interactions. Since an obvious way to improve mechanical performance of a polymer-based composite is to incorporate aligned anisotropic fillers, fibers or platelets, it becomes of interest to explore whether the same approach could benefit the electric performance. For example, it was hypothesized that in polyamide composites, aligning nanosilicate fillers perpendicular to the film surface leads to improved partial discharge properties.[15] In a different approach, the addition of high aspect ratio nanofillers arranged parallel to the thickness of a dielectric film, can provide an optimized distribution of traps and scattering centers that, in turn, can provide resistance to electric treeing inception and improve the breakdown strength across such a film. Along these lines, recent investigations, including our earlier publications, indicate that the filler orientation and their spatial distribution play a vital role in determining and improving the energy storage capabilities of nanocomposites.[6,7]

It is the focus of this paper to better understand the effect of orientation of high aspect ratio fillers on the breakdown and energy storage in PE/layered-silicate nanocomposites. This particular effect remains largely unexplored, although multiple other factors (such as the effect of compatibilizers, crystallinity, electrode effects, space-charge trapping and formation, and high field conduction, to name just a few) have been varied and linked to the high field properties of such nanocomposites.

## II. EXPERIMENTAL

### A. Materials

Commercial grade polymers and fillers were used throughout this study. PE was a Dow Integral polyolefin (an 80/20 blend of LLDPE/LDPE). The layered-silicates were commercial organomontmorillonite (MMT) purchased from Nanocor, Arlington Heights (IL), with a nominal cation exchange capacity (CEC) of 1.0 meq $\mathrm{g}^{-1}$ and modified by dimethyl-dioctadecyl-ammonium. The details of the nanocomposite preparation are discussed in detail elsewhere.[21,22] Briefly, the organo-MMT was first dispersed with a twin-screw extruder at 25 wt. % inorganic loading in maleic anhydride (MAH) functionalized PE (an LLDPE-*graft*-MAH with 0.26 wt. % MAH, $\overline{M}_w = 67000$ g $\mathrm{mol}^{-1}$ and $\overline{M}_w/\overline{M}_n \simeq 6.1$). Nanocomposites were subsequently formed by dilution of these concentrates in the PE matrix in a twin-screw extruder, yielding nanocomposites various clay-filler concentrations,[21] although only concentrations of 6 and 9 wt. % of organo-MMT are measured and discussed here. Films were extruded at thicknesses of around 0.4 mm at a commercial blown-film line.[22] Since extrusion film-blowing unavoidably induces filler orientation, a set of films with "random" filler orientations were also obtained by hot pressing to a final thickness of 0.4 mm a stack of four blown-films, stacked after sequentially rotated by 22.5° relative.

### B. Instrumentation

#### 1. *Transmission electron microscopy*

A Leica Ultracut UCT microtome equipped with a cryo-attachment was used for sectioning the specimens. The microtomed samples (cross-sections) were tested under a transmission electron microscope (TEM, Jeol JEM-2010 with $\mathrm{LaB}_6$ emitter) operated at an accelerating voltage of 200 kV.

#### 2. *Wide-angle x-ray diffraction (WAXD)*

Wide-angle x-ray diffraction (WAXD) experiments were performed both in $\theta$-$\theta$ geometry in a powder diffractometer probing a single film surface, and in transmission through the films. The transmission mode WAXD was done in a Rigaku D/MAX Rapid II instrument equipped with a 2D-detector and a graphite monochromator, using a 100 $\mu$m pinhole collimator, a 127.4 mm sample-to-detector distance, and Cu $\mathrm{K}\alpha_{1,2}$ radiation (weighted average $\lambda = 1.5418$ Å). The 2D measurements are useful in determining both the diffraction basal spacings and the orientation of periodic structures in the film. The films were stacked in such a manner that the x-ray beam was 90° to the normal of the films. Corrections for polarization and oblique incidence were applied to raw data using Rigaku AREAMAX software. No corrections were applied for background scattering or instrumental broadening. Diffractometer scans (intensity vs $2\theta$, Bragg angle) were obtained by averaging of intensity over a range of $1.5° \leq 2\theta \leq 45°$, yielding excellent agreement to the powder diffraction data from the same systems. Calculated $d$-spacings for the smectic basal spacing ($d_{001}$) were estimated by applying the Bragg relationship ($n\lambda = 2d \sin\theta$) to the first order ($n = 1$) diffraction peak, around $2\theta_{001} = 2.8°$. Azimuthal profiles (intensity vs azimuthal angle, $\beta$) were recorded by integrating the diffracted intensity over a finite interval $\Delta(2\theta)$ around the Bragg angle ($2\theta_B^{hkl}$) of the relevant $hkl$ reflection. The azimuthally integrated intensities $I(\beta)$ of the intercalated tactoids (at $d_{001}$) were first corrected for background intensity (measured in each case at proximal $2\theta$ angles on either side of the diffraction peak $2\theta_B$) and were rotated to align their peak intensities at $\beta$=0, $\pi$; these $I(\beta)$ were then converted to radial intensities $I(\phi)$ [where the radial $\phi$ is the angle between the incident and diffracted beams, $\cos(\phi) = \cos(\beta)\cos(\theta_{Bragg})$]. The resulted $I(\phi)$ intensities were subsequently used to calculate the relevant order parameter for filler orientation ($S_d$) via the Hermans orientation function[27]

$$\langle \cos^2 \phi \rangle = \frac{\int_0^{\pi/2} I(\phi)\ \cos^2 \phi\ \sin \phi\ d\phi}{\int_0^{\pi/2} I(\phi) \sin \phi\ d\phi} \tag{1}$$

yielding an order parameter for the filler orientation ($S_d$):

$$S_d = \frac{3\langle \cos^2 \phi \rangle - 1}{2} \tag{2}$$

with $S_d = 0$ for randomly or uniformly oriented fillers; $S_d = 1$ when all fillers are oriented along $\beta = 0, \pi$; and $S_d = -1/2$ for fillers oriented along $\beta = \pm\pi/2$.

### *3. Dielectric relaxation spectroscopy*

DRS experiments were performed over a broad frequency ($10^{-2}$ to $10^6$ Hz) and temperature (30 to 180 °C) range. Disklike specimens, about 100 $\mu$m thick and 20 mm in diameter, were sandwiched between gold-sputtered brass electrodes and mounted on a Novocontrol ZGS Alpha active sample cell, which was connected to a Novocontrol Quatro Cryosystem for temperature stabilization ($\pm 0.1\,^\circ$C). Prior to the DRS measurements, the samples were equilibrated in the cell at ($100\,^\circ$C) for 30 min to eliminate bulk water contributions to the spectra and to facilitate similar conditions in all the systems measured. The real and imaginary parts of permittivity [$\varepsilon^*(\omega) = \varepsilon'(\omega) - i\,\varepsilon''(\omega)$, where $\omega$ is the angular frequency] were collected isothermally in order of increasing temperature. A detailed description of the data analysis has been presented elsewhere.[6,7,28]

### *4. Differential scanning calorimetry*

DSC data were collected on a thermal analysis (TA) Instruments Q200 calorimeter operated with a gas mixture of nitrogen and helium. The measured heat flow was obtained in the conventional mode at heating and cooling temperature ramps of 10 °C/min. The nominal temperature uncertainty was ±0.1 °C. For the data analysis, the TA universal analysis software was used.

### *5. Displacement-electric field loops*

High-field polarization vs electric field (D-E) loops were recorded with a modified Sawyer–Tower circuit. The samples were subjected to two successive sinusoidal waves, with frequency of 1 Hz. The polarization-electric field loops are presented according to the data from the second cycle.

### *6. Dielectric breakdown strength*

Dielectric breakdown measurements were performed on a TREK P0621P instrument. The samples were sandwiched between a one-side conducting polypropylene tape (top electrode) and a copper plate (bottom electrode). All the specimens were tested at room temperature under a dc voltage ramp of 500 V/s (more details can be found elsewhere[3,4,7]). All results were obtained under similar ambient temperature and humidity conditions.

## III. RESULTS AND DISCUSSION

### A. Structural characterization

### *1. Orientation quantification*

In order to elucidate the effect of filler orientation on the composites' dielectric response, an investigation of the composite morphology is first necessary. TEM, 2D-XRD, and DSC techniques were employed in order to assess the dispersion and orientation of the fillers in the polymer films, as well as the effect of the inorganic phase on the polymer crystallinity.

Direct observation of the fillers via bright field TEM (Fig. 1) illustrates that the as processed PE/oMMT films (via

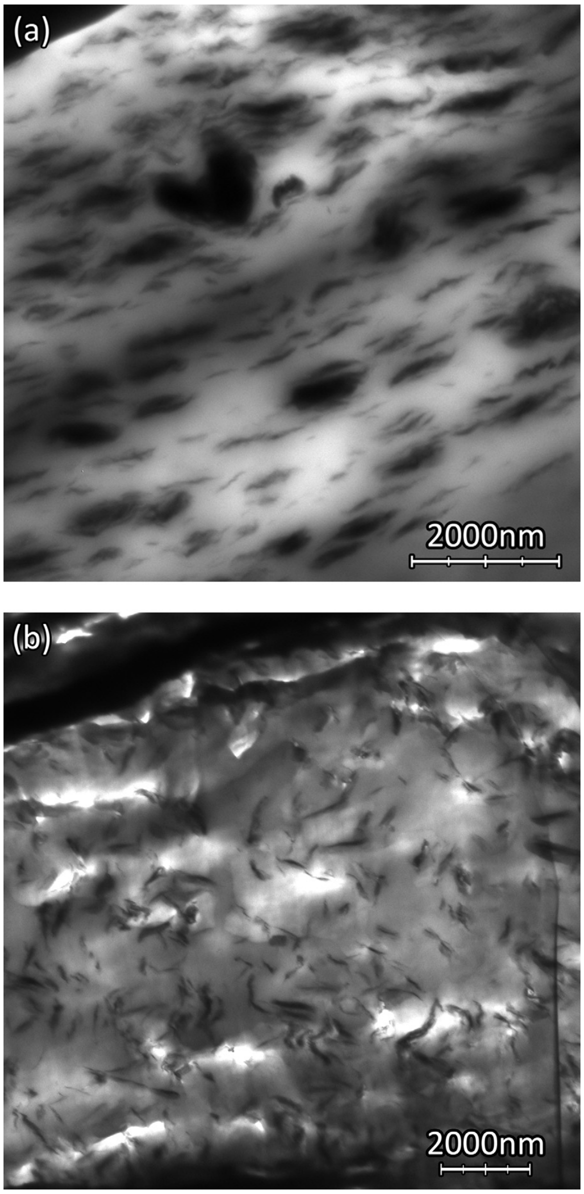

FIG. 1. TEM images showing the $\mu$m-scale dispersion of oMMT in PE nanocomposites. (a) Cross section of the films "as processed," showing a coexistence of tactoids and dispersed layers, with a definitive filler orientation along the flow direction (roughly from bottom-left to top-right corner). (b) After stacking rotated films and compression molding them, the filler orientation is markedly randomized, with no considerable loss of filler dispersion.

extrusion blow-molding) show a coexistence of tactoids—the extended dark areas in Fig. 1(a)—and well dispersed fillers—in smaller clusters consisting of a few layers down to single layers. Comparison of the as processed films with the films after stacking and hot-pressing to randomize the filler orientation [Fig. 1(a) vs Fig. 1(b)] does not reveal any substantial filler aggregation upon this additional melt-processing, i.e., the dispersed filler clusters remain at comparable sizes (a few individual layers each) and remain well-dispersed throughout the PE matrix. This behavior is a direct consequence of the thermodynamically favorable dispersion of the oMMT fillers, mediated by the existence of the LLDPE-*graft*-MAH polymer,[29] and is also reflected in the powder x-ray diffraction of the respective systems [Fig. 2(a)]. Namely, comparison of the powder XRD between the two films does not show any qualitative changes in the intercalated filler diffraction ($2\theta_{001} \simeq 2.8°$ and $2\theta_{002} \simeq 6.7°$), or in the PE crystal ($15° < 2\theta < 30°$); WAXD only shows quantitative differences, such as an increased diffracted intensity and a peak sharpening for both the 001 and 002 reflections in the as processed films, which are consistent with higher intercalated populations being parallel to the film surface probed by the WAXD, that is, higher filler orientation (vide infra). Finally, on this last point, regarding the filler orientation, it is evident from the TEM observation that the as processed films [Fig. 1(a)] possess a high degree of filler orientation that align parallel to the film surface, largely following the direction of the flow [bottom right to top left in Fig. 1(a)], whereas after stacking and hot-pressing this filler orientation is mostly lost [Fig. 1(b)]. A more quantitative analysis of the filler orientation was done with two-dimensional transmission WAXD through azimuthal analysis of the filler diffraction peaks [Figs. 2(b) and 2(c)].

Specifically, using two-dimensional WAXD in transmission mode through the films, we collected the two-dimensional diffraction patterns for both the montmorillonite basal reflections [the high intensity features near the beam-stop in Fig. 2(b)], as well as the polymer crystalline diffractions at higher angles (the outer bright “ring” corresponds to the 110 and 200 PE reflections at $2\theta \simeq 21.5°$ and $23.9°$). The 2D patterns match closely the powder XRD [shown in Fig. 2(a)] when integrated radially, and can additionally provide a quantitative measure of filler alignment via Herman’s orientation function [Eq. (1), and the respective order parameter, $S_d$, Eq. (2)] when the relevant diffraction peaks are integrated azimuthally: for example, in Fig. 2(c) we show the azimuthal diffracted intensities for the montmorillonite 001 intercalated peaks at $2\theta \simeq 2.8°$). It is evident that the as processed films possess a high degree of filler orientation (denoted “oriented PE/mmt”), which manifest as strong reflection-lobes at $\beta = 0, \pi$

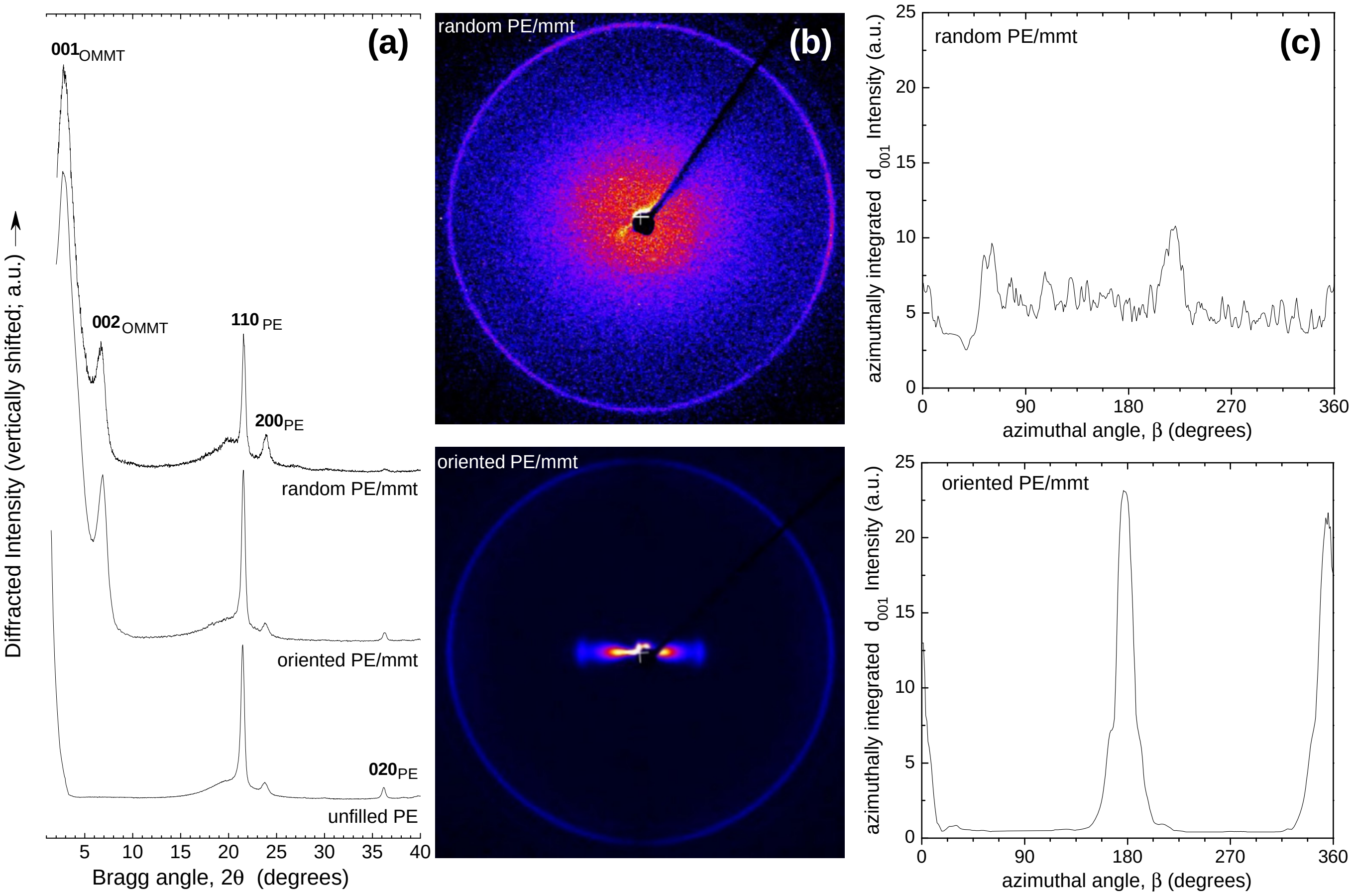

FIG. 2. (Color online) Wide-angle x-ray diffraction of the PE/MMT nanocomposites. (a) Comparison of the powder XRD for unfilled PE and its nanocomposites with oriented and random MMT fillers. (b) 2D XRD patterns for nanocomposites with random (top) and oriented (bottom) fillers (the pseudocolor denotes diffracted intensity, and the white cross the calculated beam center). (c) Azimuthal integrated intensities, $I(\beta)$, of the $d_{001}$ diffraction peak for the 2D XRD patterns shown in (b).

[Fig. 2(c)], whereas after stacking and hot-pressing there is a marked loss of this orientation (systems denoted as "random PE/mmt," with the azimuthal intensity being almost constant across the $\beta$ angle, Fig. 2(c); the features at $\beta \simeq \pi/4$, $\pi/3$, and $5\pi/4$ are due to beam stop scattering). Further, calculating the $S_d$ order parameters for these $d_{001}$ data we got a $S_d = 0.80$ for the oriented films ($S_d = 1$ corresponds to perfect filler alignment parallel to the flow direction) and $S_d = 0.02$ for the random films. Comparatively, calculating the same order parameter for the strongest PE diffraction peak [110 peak at $2\theta \simeq 21.5°$, which is the outer ring in Fig. 2(b)] gave $S_d$ of 0.21 and 0.01 for the oriented and the random films, whereas for the background intensity $I(\beta)$ at $2\theta \simeq 9°$ it is $S_d$ of 0.01 and $-0.02$ for the oriented and the random films, respectively. These results clearly denote that the PE/oMMT films as produced by extrusion blow-molding resulted in a high degree of filler orientation [as also observed directly via TEM, Fig. 1(a)], whereas stacking relatively-rotated such films and hot-pressing them results in a film with well randomized filler orientation. As expected, the PE polymer crystals remain largely nonoriented in both these systems, with a moderate only filler-orientation order parameter ($S_d$ of 0.21) for the strongest PE diffraction peak; however, the extra high temperature process of hot-pressing and subsequent cooling may have altered the polymer crystallinity (cf. crystal fraction). Since changes in polymer crystallinity can influence the response of these systems to electric fields, it is important to quantify any such changes via DSC.

### *2. DSC studies*

The PE in this study is a semicrystalline polymer blend of LLDPE and LDPE, containing both crystalline and amorphous domains. Figure 3 compares the melting endothermic and crystallization exothermic peaks for the 6 wt. % nanocomposites with random and oriented fillers. The degree of crystallinity (crystal fraction, $\phi$) was calculated using $\phi = \Delta H_m / \Delta H_m^o$, where $\Delta H_m$ is the melting enthalpy measured from the area under the curve of the melting endotherm and $\Delta H_m^o$ is the enthalpy of fusion of 100% crystalline PE ($\Delta H_m^o = 290$ J/g for $\phi = 1$). The two calculated values were found to be 40% and 38% for the nanocomposites with aligned/oriented and with random fillers, respectively. However, a decrease of approximately 3 °C is observed in the melting temperature of the PE for the composite with random fillers. This small difference in $T_m$ most probably reflects differences in the thermal history that were not erased by the first DSC scan, or differences in the composites' thermal conductivities; however, similar behavior has been reported before in clay composites and was attributed to changes in the interactions between the maleic anhydride and the clay particles.[30] A definitive explanation for this behavior cannot be provided with the data at hand, and requires further experimental investigation; however the melting point difference is far too small to cause any marked effects in the comparative electric field performance of these two nanocomposites. In the cooling cycle, the cold crystallization peaks are of the same area in both samples, the two systems also show the same enthalpy of crystallization, although the peak in random-filler composite is slightly broader, probably reflecting a broader distribution in the size of the spherulites. It is generally believed that the electronic mobility through the crystalline regions of polyethylene is larger than through the amorphous regions.[31]

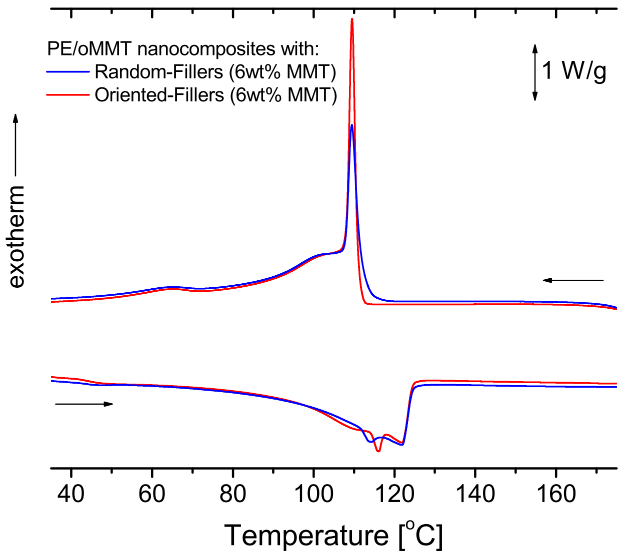

FIG. 3. (Color online) DSC traces of the LLDPE/LDPE-based nanocomposites with 6 wt.% oMMT (heating/cooling rate: 10°C/min).

Thus, the similar crystallinities of the two types of nanocomposites, as discussed above, together with the similar filler dispersions, as discussed in the previous paragraph, denote that the two selected films provide a consistent platform to compare the electric-field behavior of these nanocomposites as a function of the filler orientation only (vide infra).

## B. Dielectric measurements under low electric field

Although our systems vary macroscopically only with regards to their filler orientation/alignment, both these systems contain a number of different nanoscale structures and phases: These structures consist of amorphous and crystalline PE regions, fillers, filler/polymer interfaces, and regions with inclusions of the minority LLDPE-*g*-MAH polar polymer; a schematic depiction of the our system is given in Fig. 4. In particular, the polar LLDPE-*g*-MAH copolymers are expected to be predominately in contact with the oMMT

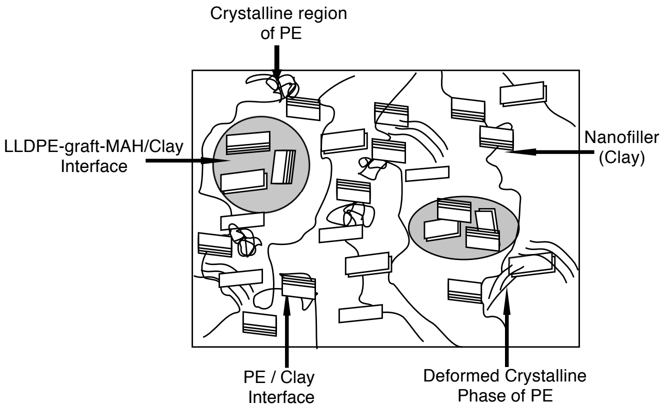

FIG. 4. Schematic depiction of the morphological features in the PE/LLDPE-*graft*-MAH/oMMT system.

fillers,[21,29] mixed with the nonpolar LDPE and LLDPE polymers,[21,22] and most probably can cocrystallize with the matrix PE.[22] Regarding the response of these films to applied electric fields, and comparing to the respective unfilled PE, any increased conductivity can be associated to the high filler loading along with the presence of polar MAH groups. Low field dielectric measurements can be effectively utilized to study and understand the dielectric and dynamic properties of the polymer-filler interfaces, in order to better understand the high electric field performance. Dielectric measurements were performed on films of unfilled polyethylene (PE), and on two nanocomposite films (based on the same PE and including MAH-polymer and MMT fillers) that only differ in their filler alignment.

Figure 5 illustrates the frequency dependence of the low field dielectric losses [$\varepsilon''(\omega)$, arising due to the conductivity and due to space-charge present in these systems] measured at room temperature. All the composites were found to exhibit similar losses (slightly higher for the 9 wt.% in oMMT, compared to the 6 wt.%) and are approximately two orders of magnitude higher compared to those of the respective unfilled PE. The observed ac conductivity also showed a similar behavior across all systems, effectively the same for all nanocomposite films and about two orders of magnitude higher than the unfilled PE [Fig. 5(b)]. Despite the increased ac conductivity in the nanocomposites, the filler orientation has little effect on the $\varepsilon''$ or the $\sigma_{ac}$. The two relaxations present in the dielectric losses [Fig. 5(a)] can be ascribed to two different processes: First, an interfacial polarization at low frequencies due to the trapping of space-charges [enhanced by the presence of fillers and polar MAH groups, denoted as "slow relaxation" in Fig. 5(a)]. As indicated before, for thermodynamic reasons the MAH phase is expected to exist predominately around the inorganic fillers, thus contributing to the slow relaxation associated with trapped space-charge (cf. interfacial polarization). A second process [weaker mode at higher frequency, denoted as "fast relaxation" in Fig. 5(a)] is most probably related to the orientation polarization associated with the polar LLDPE-*graft*-MAH chains, and which is expected to occur at higher frequencies than the interfacial polarization (since this faster mode is arising from the movement or reorientation of dipoles present in the MAH polymers[32–35]). This faster mode will not be discussed further, since the current study focuses on the space-charge dynamics and their correlation with the high electric field properties of the composites. Also, it was observed that the maximum frequency of both the abovementioned processes is independent of the morphology and filler weight fraction, suggesting that all samples have equally good dispersions (similar extents of exfoliated structures dispersed uniformly in the composites) and with their MAH phases similarly distributed in the composite and around the fillers.

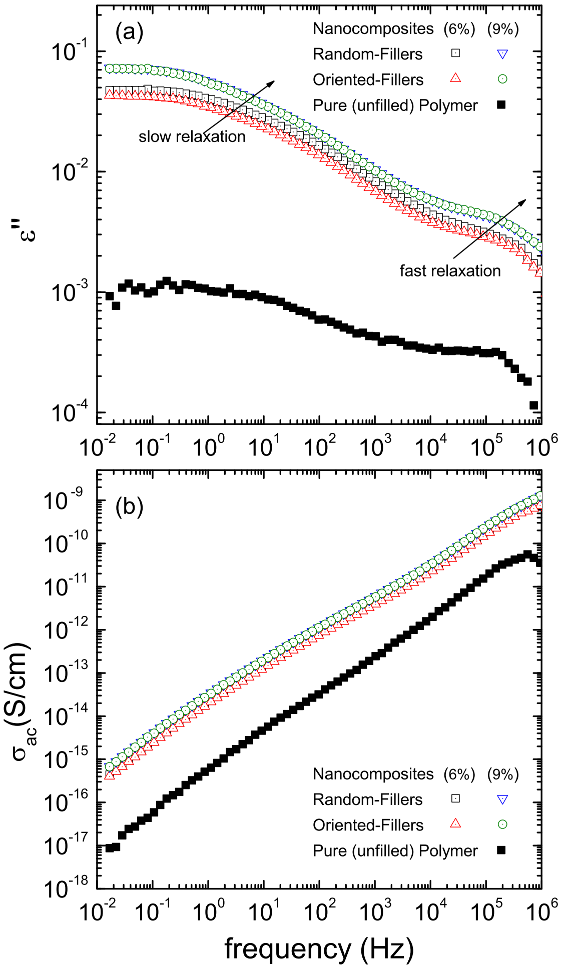

FIG. 5. (Color online) Low electric field behavior, broadband dielectric relaxation spectroscopy (DRS) data: (a) Dielectric losses of the pristine PE blend and of its PE/oMMT nanocomposites at 6 and 9 wt.% oMMT. (b) The corresponding ac conductivity plots.

Since space-charge mechanisms are extremely important to the high electric field behavior, the time scale of the space-charge was also followed at higher temperatures, and a representative comparative plot for the 9 wt. % organo-MMT nanocomposite is presented in Fig. 6. A bimodal relaxation is present in all the composites and for the analysis of this mode the permittivity experimental data were fitted by the superposition of two Havriliak–Negami expressions

$$\varepsilon^*(\omega) = \varepsilon_\infty + \sum_{i=1}^{2} \frac{\Delta\varepsilon_i}{\left[1+\left(i\omega\tau_{0,i}\right)^{1-\alpha_i}\right]^{\beta_i}} \qquad (3)$$

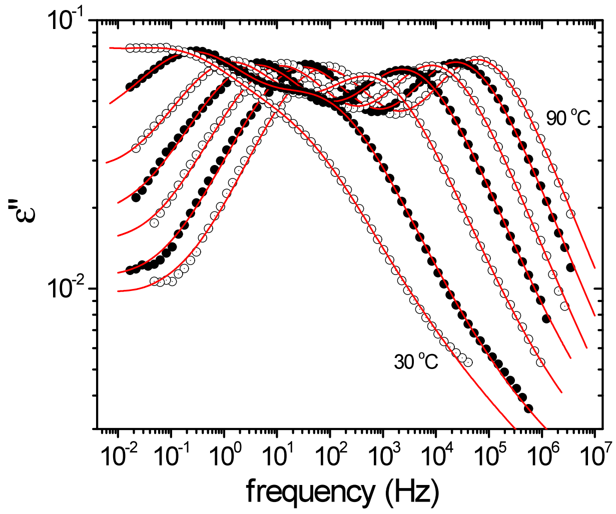

FIG. 6. (Color online) Dielectric losses for the linear low density polyethylene with 9 wt.% organo-MMT. The relaxations are due to the space-charge. The temperature range is 30 to 90 °C in steps of 10 °C. The best fitting curves of Eq. (3) to the experimental data are also presented.

TABLE I. Best-fit parameters for the space-charge relaxations in Fig. 6.

| $T$ (°C) | $\alpha_{lf}$ | $\beta_{lf}$ | $\Delta\varepsilon_{lf}$ | $f_{\max}^{\text{slow}}$ (Hz) |
|---|---|---|---|---|
| Low frequency (slow) relaxation | | | | |
| 30 | 0.53 | 1 | 0.22 | 0.16 ± 0.01 |
| 40 | 0.45 ± 0.01 | 1 | 0.24 ± 0.01 | 0.26 ± 0.01 |
| 50 | 0.41 ± 0.01 | 1 | 0.21 ± 0.01 | 1.28 ± 0.03 |
| 60 | 0.43 ± 0.01 | 1 | 0.24 ± 0.01 | 3.77 ± 0.12 |
| 70 | 0.43 ± 0.01 | 1 | 0.24 ± 0.02 | 10.83 ± 0.33 |
| 80 | 0.42 ± 0.01 | 1 | 0.24 ± 0.02 | 28.53 ± 0.87 |
| 90 | 0.41 ± 0.02 | 1 | 0.24 ± 0.02 | 69.87 ± 2.10 |
| High frequency (fast) relaxation | | | | |
| $T$ (°C) | $\alpha_{hf}$ | $\beta_{hf}$ | $\Delta\varepsilon_{hf}$ | $f_{\max}^{\text{fast}}$ (Hz) |
| 30 | 0.44 ± 0.02 | 1 | 0.15 ± 0.01 | 22 ± 3 |
| 40 | 0.45 ± 0.02 | 1 | 0.15 ± 0.01 | 76 ± 9 |
| 50 | 0.42 ± 0.01 | 1 | 0.21 ± 0.01 | 659 ± 78 |
| 60 | 0.39 ± 0.02 | 0.93 ± 0.11 | 0.22 ± 0.01 | 2959 ± 482 |
| 70 | 0.38 ± 0.02 | 0.90 ± 0.11 | 0.24 ± 0.01 | 9919 ± 1628 |
| 80 | 0.38 ± 0.02 | 0.92 ± 0.12 | 0.25 ± 0.01 | 28036 ± 4856 |
| 90 | 0.37 ± 0.02 | 0.94 ± 0.13 | 0.25 ± 0.02 | 68757 ± 12823 |

where $\omega(=2\pi f)$ is the angular frequency; $\Delta\varepsilon = \varepsilon_s - \varepsilon_\infty$ is the dielectric relaxation strength, $\varepsilon_s$ and $\varepsilon_\infty$ are the low and high frequency limits of the $\varepsilon'(\omega)$; and $\tau_{0,i}$ is the relaxation time of the $i$ mode, associated with each mode's characteristic frequency $f^i_{\max}$. The parameter values of the best-fits are provided in Table I. The shape of the loss peak is described by the $\alpha$ and $\beta$ parameters, which are associated to the slopes of the $\varepsilon''(\omega)$ function at the low and high frequency limit with respect to the maximum frequency of each mode.

Taking into account that no relaxation is evident for the unfilled PE in the same temperature range (Fig. 7), we may safely assign the origins of the two modes present in the nanocomposites films (Fig. 6) to relaxation mechanisms arising from the MMT fillers and the MAH-polymer. Also, the absence of any dc conductivity in the dielectric spectra manifests that these diffusive type of motions are topologically restricted and limited by the presence of neighboring polymer/oMMT interfaces, i.e., they correspond to a genuinely trapped space-charge. Thus, the slower relaxation is the interfacial polarization, cf. Maxwell–Wagner effect; whereas, the faster mode should relate to the polarization of domains containing MAH groups, cf. it should arise from the restricted mobility of ions present at LLDPE-*graft*-MAH/oMMT interfaces, i.e., short length scale motions of the space-charge, probably localized mostly at the polymer/oMMT interfaces. The slow (lower frequency) losses can be ascribed to a longer length scale motion of the space-charge, indicating that at these time scales the space-charge can escape from the polymer/oMMT interface (trap) and diffuse through the bulk polymer phase; this diffusion of the space-charge between the neighboring polymer/oMMT interfaces is significantly slower (∼1000 times) than the short length scale motions of the space-charge within an interface, in agreement with what was observed before for space-charge dynamics in epoxy/MMT nanocomposites.[3,4]

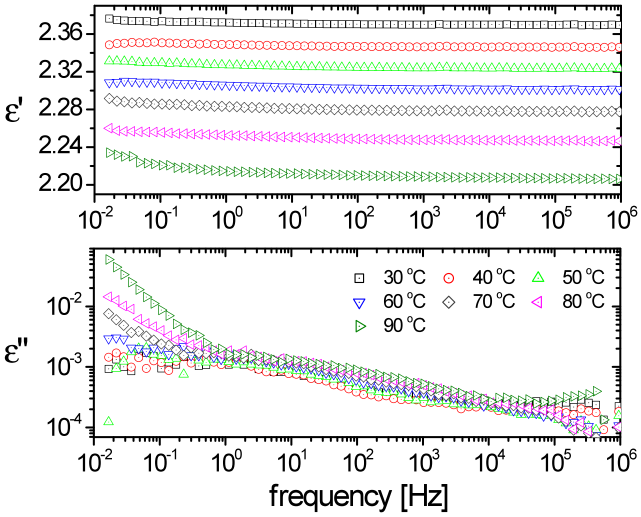

FIG. 7. (Color online) Real ($\varepsilon'$) and imaginary ($\varepsilon''$) parts of the permittivity for the unfilled PE. No relaxation process is seen neither in the imaginary or the real part. The slight decrease in the ($\varepsilon'$) values upon temperature increasing can be attributed to changes in the local density due to onset of melting as well as due to water evaporation at elevated temperatures.

The parameters of the best fit of Eq. (3) to the experimental data in Fig. 6 are summarized in Table I. The shape parameters for the long range motion of the space-charge (slow relaxation, entire temperature range) and for the short range motion of the space-charge (fast relaxation, in the temperature range 30–50 °C) indicate that both modes are described by Cole–Cole distributions ($\beta = 1$). Furthermore, the symmetrical broadening of the loss peaks with respect to a Debye peak ($\alpha = 0$, $\beta = 1$) is similar for both modes (similar $\alpha$ values, Table I); this indicates that the spatial distribution of the corresponding local environments, where these modes are located, are of similar symmetry, an indication which is consistent with a good filler dispersion. Furthermore, the broadness of the loss peak—which corresponds to a distribution in the respective relaxation times—can be attributed to local heterogeneities, such as the existence of regions with exfoliated or agglomerated oMMT fillers. Interestingly, the fast space-charge relaxation at high temperatures (60–90 °C) becomes asymmetric and is described by a Havriliak–Negami expression ($\beta \sim 0.9$). This deviation from the Cole–Cole reflects a temperature-induced change in the corresponding mobility of the space-charge, which most probably relates to structural changes of the polymer/oMMT interfaces at the higher temperatures, for example, onset of melting of the MAH-containing phases. Finally, the dielectric relaxation strengths ($\Delta\varepsilon$) of both modes are comparable, indicating that the number density of the dipoles contributing to each mode and their mean dipole moment are similar. All the above behaviors are consistent with the existence of a "coupling" between the two modes sharing a common space-charge carrier population: i.e., the same space-charge carriers relax in the vicinity of the oMMT fillers or within filler/polymer interfaces at high frequencies (short time scales) and the same populations also diffuse to neighboring interfaces at longer time scales (lower frequencies).

Finally, it is informative to examine the temperature dependence of the two relaxation times: The characteristic frequencies $f_{\max}$ for both modes are plotted versus temperature in Fig. 8, and are evidently described well by Arrhenius processes $[f^i_{\max}(T) = f^i_\infty \exp(-E^i_A/k_BT)$, where $f_{\max}$ is the relaxation rate of process $i$ and $f_\infty$ is the respective relaxation

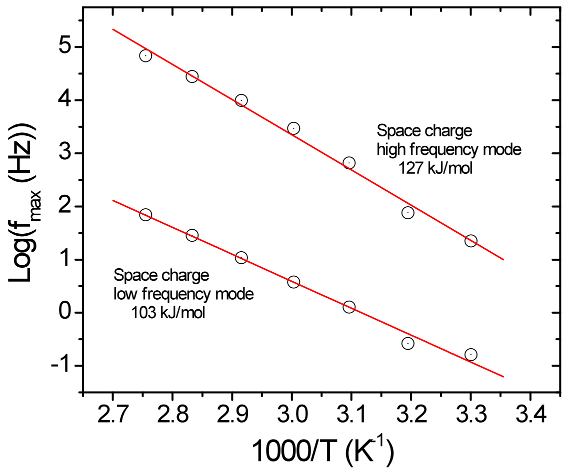

FIG. 8. (Color online) Arrhenius plot for the relaxation rates ($f_{max}$) of the two space-charge modes observed, cf. high and low frequency relaxations in Fig. 6 and Table I.

rate at the high temperature limit, $E_A$ is the corresponding activation energy, and $k_B$ is the Boltzmann constant]. Fitting to an Arrhenius equation, the resulting activation energies for the fast (high frequency) and slow modes were 127 and 103 kJ/mol, respectively. These rather high values of activation energy are typical for ion conduction mechanisms, and further support the postulation that the observed modes are due to space-charge effects. These activation energies result from the space-charge electrostatic interactions with the polar MAH/MMT interfaces and with the charged MMT fillers;[32,33] thus, in agreement with the fit results, it is expected that the space-charge motion within the polar interfaces or in the vicinity of the fillers (fast mode) should be characterized by a higher $E_A$ than when diffusing between neighboring interfaces (low frequency relaxation), where it experiences lower electrostatic barriers. The space-charge introduced in the system by the incorporation of the fillers, will be discussed further in correlation with the electric breakdown properties of the samples.

## C. High Field Dielectric Properties

### 1. *Displacement-electric field loops*

Fillers with high permittivity embedded in polymer matrices of lower permittivity create strong electric field inhomogeneities at the polymer/filler interfaces. With increasing extent of such interfaces in a composite material, such as composites with nanometer-scale fillers, these interfacial dielectric inhomogeneities can dictate the macroscopic behavior of the material, especially in controlling the ac and dc conductivities and the space-charge formation.[3,4,6] All these factors concurrently determine the dielectric breakdown strength of a material and, thus, its energy storage capabilities. In order to quantify and understand the behavior of recoverable energy density in the present thermoplastic nanocomposites, displacement-electric field loops were obtained as a function of applied field (shown in Fig. 9). The widening (or opening) of these loops depicts a deviation from the linear behavior of the dielectric displacement versus the electric field and is related to the magnitude of losses (space-charge, conduction, etc.) present in the system. A linear behavior of polarization with applied field was observed in the unfilled PE matrix at all field levels, denoting a well-defined/proper dielectric material. The nanocomposites show higher losses in the D-E loops, denoting an easier development of space-charge at high fields in these systems compared to the unfilled PE. Also, the nanocomposite with randomly oriented fillers showed markedly higher losses (broader D-E loop) than the nanocomposite containing oriented fillers; this behavior can be intuitively rationalized since oriented-filler samples are expected to provide more ordered trapping centers and more efficient scattering for the injected charge, thus obstructing its ability to traverse the sample to the opposite electrode. This obstruction should be less for randomly dispersed fillers, even when they are in the form of high aspect ratio clays, rendering a nanocomposite with no filler orientation more lossy at high fields than a respective materials with oriented fillers. It must also be noted that the filler geometry is very important here: individual clay particles, as well as clay agglomerates, have an elongated ellipsoidal shape and, since they define the polar phases in the composite, are expected to give rise to anisotropic carrier mobilities. Thus, high field conduction and breakdown strengths are very likely to also be affected by the fillers' orientation within the composite, in contrast to the insensitivity exhibited at low electric fields (vide infra).

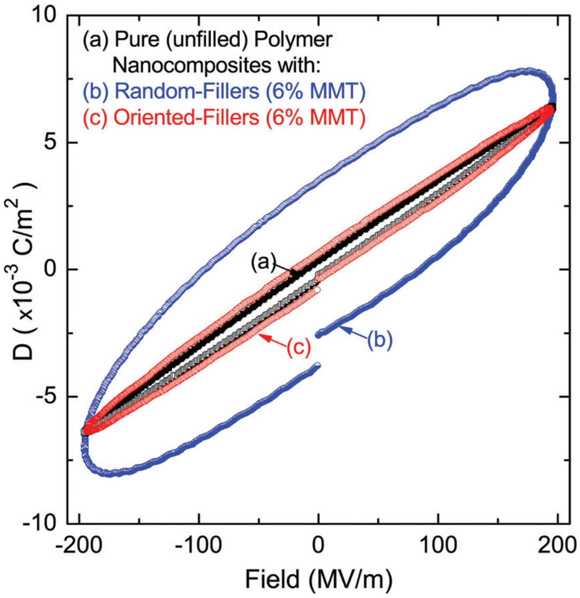

FIG. 9. (Color online) Displacement-electric field (D-E) loops showing the evolution of high field losses present in PE nanocomposites; the effect of filler orientation is clearly depicted by the marked widening of the loop.

### 2. *Energy density*

The recoverable energy density at any field can be obtained by integration of the area between the D-E loop curve and the corresponding ordinate. In Fig. 10 the calculated recoverable energy densities are presented as a function of applied field; the "maximum" recoverable energy density corresponds to the electric breakdown strength ($E_{BD}$) of each material (vide infra). The unfilled PE data were extrapolated, assuming a monotonic increase in the losses, to its dc breakdown field level. It is evident that the addition of oMMT

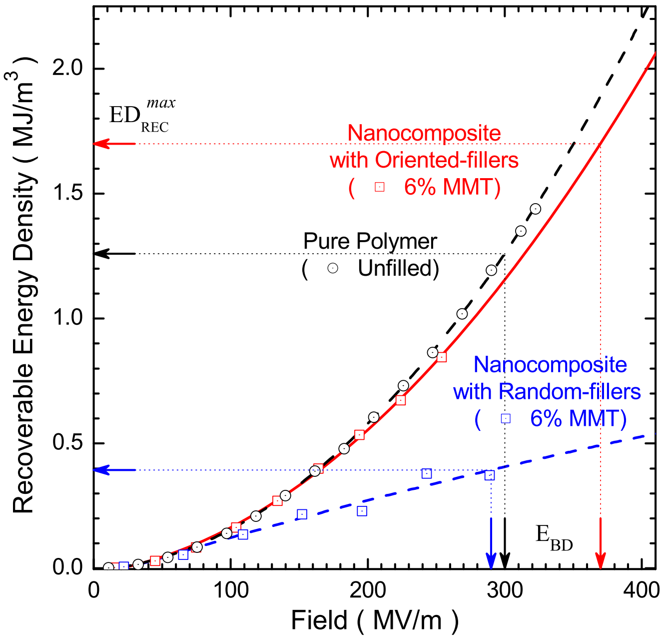

FIG. 10. (Color online) Calculated recoverable energy densities versus ac field, for the various systems studied. The vertical arrows denote the dc electric breakdown strength of each material and the horizontal arrows denote the corresponding ("maximum") recoverable energy density. There is a clear marked improvement in recoverable energy density upon filler orientation.

nanofillers with a random dispersion (no orientation) markedly decreases the recoverable energy density of PE. However, incorporation of the same fillers but with a controlled orientation results in an appreciable improvement in recoverable energy density, when compared to the respective unfilled PE. This enhancement for the aligned-filler nanocomposites is consistent with, and probably arises from, the reduction in the associated losses present at high fields along with an increased field endurance. In Fig. 11 we demonstrate the energy storage efficiency of pure (unfilled) PE and of PE nanocomposites (with oriented and randomly distributed fillers). The oriented-filler nanocomposite and the unfilled PE exhibit similar performances in efficiency, whereas, the randomly dispersed filler nanocomposites exhibit a considerably poorer performance, further signifying the advantages of oriented high aspect ratio fillers within a nanocomposite. It is possible that the slightly larger dielectric losses seen in all the oriented samples are the result of high field generated space-charge, primarily due to "impurity" ions, such as free dioctadecyl-ammonium or chloride left over from the compatibilization process. In summary, the losses present in the random-filler system, e.g., space-charge, high field conduction, etc., all contribute to a decrease in the amount of recoverable energy density and an associated degraded efficiency.

### *3. Dielectric breakdown*

The characteristic electric breakdown strength of the composites is analyzed within the framework of Weibull statistics, using a mean sample size of 15. A complete description of the methods and analysis is given in our earlier publications.[3,4,6] The Weibull parameters $\alpha_W$ and $\beta_W$, essential for the complete characterization of the material, were calculated from the slope and the ordinate at the origin and are represented in Fig. 12. The characteristic breakdown strength $\alpha_W$ was found to be strongly affected by the filler orientation in the nanocomposite samples. The Weibull modulus $\beta_W$ quantifies the scattering in the experimental data and a higher value of $\beta_W$ represents less scattering. The calculated $\beta_W$ values are found to be 21, 19, and 7 for the unfilled PE, the 6 wt.% nanocomposite with oriented fillers, and the 6 wt.% randomly dispersed filler nanocomposite, respectively; whereas, for the same systems the characteristic dielectric breakdown strengths ($\alpha_W$) were 300, 370, and 290 MV/m, respectively (Fig. 12). The distribution of breakdown strengths does not significantly change for the nanocomposites when the filler loading is increased from 6 to 9 wt.% filler (the same behavior was also seen before for

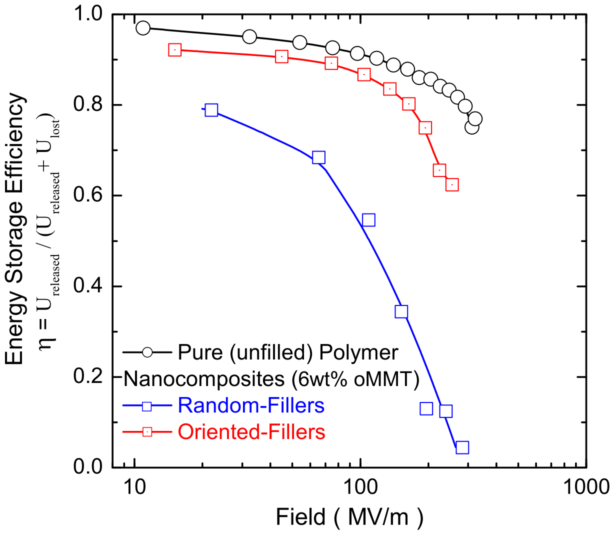

FIG. 11. (Color online) Observed energy storage efficiencies versus ac field, calculated using the data presented in Figs. 9 and 10.

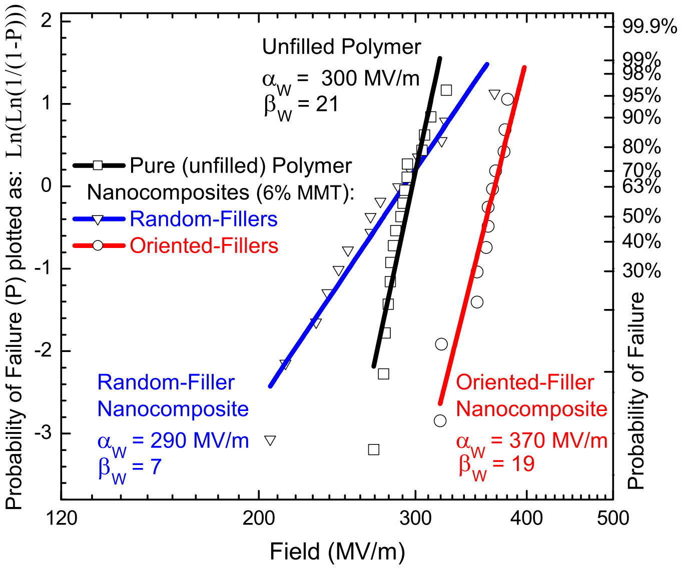

FIG. 12. (Color online) Experimentally observed dielectric breakdown strengths, plotted as a probability of failure versus applied electric dc field (Weibull statistics). The Weibull fitted lines and the corresponding parameters are also shown for a pure (unfilled) polymer, for a nanocomposite with random fillers, and for a nanocomposite with oriented fillers. There is a strong effect of the filler orientation on the breakdown behavior of the composites, which results in marked improvement of the high field breakdown strength for the oriented-filler nanocomposites.

epoxy/MMT nanocomposites[3,4]). This leveling-off of the breakdown strength at higher loadings of oMMT indicates that the 6 wt.% oMMT composites already reached the onset of percolation for the interfacial regions, and emphasizes the significant role of filler dispersion and orientation in determining the dielectric strength.

Beyond the impressive improvement in the $\alpha_W$ value of the breakdown strength, which corresponds to the electric field for 63.2% probability of failure, the distributions of the breakdown failures are also very interesting: The $\beta_W$ shape parameter for the random-filler nanocomposite is 7, and increases to 19 for the oriented-filler nanocomposite, indicating that the latter is more homogeneous and exhibits fewer defects,[36] comparable to the behavior of the unfilled polymer matrix ($\beta_W = 21$, Fig. 12). Similarly, focusing on the lower field failures, the random-filler nanocomposite shows a considerable drop in breakdown strength compared to the unfilled PE, whereas the oriented-filler nanocomposite shows a dramatic improvement in breakdown strength compared to the unfilled PE. For example, the breakdown strength that corresponds to a 10% probability of failure is 325 MV/m for the oriented-filler nanocomposite, compared to 270 MV/m for the unfilled PE, and to 210 MV/m for the random-filler nanocomposite. Even more importantly, the complete population of failures for the oriented-filler nanocomposite lies at higher fields than the value the corresponds to 95% probability of failure for the unfilled polymer (Fig. 12). These considerations have very important implications for the reliability and the lifetime of energy storage devices. Although the present study focused on the dielectric materials (that is, it did not consider electrode design, graceful failure, and mean time between failures[36]) the breakdown distributions are indicative of a worst case behavior from an application viewpoint, and still the observed behavior is pretty good.

The distinct population of low breakdown strength failures observed in randomly dispersed PE/oMMT nanocomposites suggests that the nonordered/random filler particles may be acting as defect initiators that promote electron tree inception. In contrast, the samples with oriented-fillers exhibit the highest breakdown strengths, consistent with the postulation that oriented fillers should frustrate the progress of electrical treeing, by offering more tortuous paths to treeing and possessing larger populations and more structured (pseudoperiodic) scattering centers. This situation will lead to higher probabilities for the hot electron scattering, thus limiting their energies. Furthermore, any fillers with a perpendicular (to the measuring field) orientation may provide higher resistance to filamentary thermal and electromechanical breakdown events, especially for these high aspect ratio oMMT fillers. In addition, the incorporation of oMMT fillers in PE also results in high improvements in the mechanical properties of the material (i.e., an 177% increase in modulus with a retention of toughness[22]) which may further contribute to improving their high electric field strength, e.g., by spreading the local thermal and electrical stresses over larger material volumes. Interestingly, if one accounts for the effects of oriented platelet filler particles on the heat transport and barrier properties of a nanocomposite, it is appropriate to think of an anisotropic intrinsic thermal conductivity within these nanocomposite materials that can further influence electric field breakdown events. Since the breakdown process will ultimately involve electrical and thermomechanical activity, it becomes difficult to pinpoint the exact underlying mechanisms. Hence, a thorough knowledge of macroscopic parameters such as Young's modulus, thermal conductivity, electrical conductivity, and space-charge profile, as well as their directional anisotropies, are needed to account for all macroscopically observed results.

## IV. CONCLUSIONS

We investigated the effect of high aspect ratio organo-montmorillonite (oMMT) fillers on the electrical properties of PE, in particularly focusing on the filler orientation effects. Toward this end, we compared unfilled PE with two PE/oMMT nanocomposites, which only differ in the alignment/orientation of the platelet-type nanofillers across the dielectric film: Comparative characterization showed that the two type of nanocomposites possess essentially the same composite morphology (filler dispersion) and very similar crystallinities (similar crystal fraction, and the same melting point and crystal structure), whereas 2D-XRD and TEM showed that in one case the fillers are highly aligned parallel to the film surface (oriented systems, with filler order parameter $S_d = 0.8$) and the other containing fillers with random orientation (random systems, $S_d = 0.02$).

Upon electrical characterization of these systems, it was found that at low electric field the two PE/oMMT nanocomposites were characterized by essentially the same dielectric properties [$\varepsilon'(\omega)$, $\varepsilon''(\omega)$, and $\sigma_{ac}(\omega)$], and both systems were about 100 times higher than the respective unfilled PE films in $\varepsilon''$ and $\sigma_{ac}$. Both composites showed two dielectric relaxations, that were absent in the unfilled PE, and related to space-charge dynamics—either as charge build-up in polarized domains (Maxwell–Wagner) or as charge dynamics within the filler interfaces. At high electric fields however, the difference in filler orientation significantly affected their dielectric properties, showing marked difference between the composites with random and oriented fillers. Specifically, the nanocomposites with oriented fillers exhibited consistently higher electric breakdown strengths, compared to the unfilled PE films, which, in turn, showed superior performance than the random filler nanocomposites. It is very noteworthy, that for two nanocomposites that differ only in the filler alignment, oriented filler structures showed an improvement in breakdown strength compared to the unfilled polymer matrix, whereas random filler orientation showed a deterioration. This behavior is in concert with the expectations that aligned fillers optimize the electric field distribution inside the nanocomposites and, more importantly, that aligned fillers would particularly affect the electrical breakdown tree inception and propagation across a dielectric film. Independent of the underlying mechanism, this study definitively shows that the orientation of oMMT-platelet nanofillers perpendicular to the electric field is evidently essential in improving the strength and in impeding space-charge losses. Finally, still considering the high electric field behavior, nanocomposites with aligned fillers showed a marked improvement in recoverable energy density of the polymer, whereas random fillers resulted again in a deteriorated performance. As a future outlook, it can be concluded that the degree of filler orientation can be tailored—together with the PE/oMMT interface nature and the mechanical properties—to improve the electrical breakdown strength and the recoverable energy density in thermoplastic nanocomposite systems and, thus, can lead to enhanced high-performance polymer-based materials for insulation and for energy storage.

## ACKNOWLEDGMENTS

This work was supported by the office of Naval Research (Grant No. MURI-00014-05-1-0541). G.P. and E.M. acknowledge additional financial support by the National Science Foundation (NSF Grant No. DMR-0602877). The authors are indebted to Dr. Jin-Young Huh (Manias Group of ca. 2004) for the preparation of the oriented-filler nanocomposites.

[1] L. An, S. A. Boggs, and J. P. Callame, IEEE Electr. Insul. Mag. (USA) **24**, 5 (2008); G. Blaise and W. J. Sarjeant, IEEE Trans. Dielectr. Electr. Insul. **5**, 779 (1998); I. Burn and D. M. Smyth, J. Mater. Sci. **7**, 339 (1972).

[2] G. R. Love, J. Am. Ceram. Soc. **73**, 323 (1990).

[3] G. Polizos, V. Tomer, E. Manias, and C. A. Randall, J. Appl. Phys. **108**, 074117 (2010).

[4] V. Tomer, G. Polizos, E. Manias, and C. A. Randall, J. Appl. Phys. **108**, 074116 (2010).

[5] M. Rabuffi and G. Picci, IEEE Trans. Plasma Sci. **30**, 1939 (2002).

[6] V. Tomer, C. Randall, G. Polizos, J. Kostelnick, and E. Manias, J. Appl. Phys. **103**, 034115 (2008).

[7] V. Tomer and C. A. Randall, J. Appl. Phys. **104**, 074106 (2008).

[8] P. Tiemblo, M. Hoyos, J. Gomez-Elvira, J. Guzman, N. Garcia, A. Dardano, and F. Guastavino, J. Phys. D **41**, 125408 (2008).

[9] S. Hui, T. K. Chaki, and S. Chattopadhyay, Polymer Eng. Sci. **50**, 730 (2010).

[10] T. J. Lewis, J. Phys. D **38**, 202 (2005).

[11] J. Nelson and Y. Hu, in *Proceedings of the 2004 IEEE International Conference on Solid Dielectrics (ICSD 2004)* (IEEE Inc., Piscataway, NJ, 2004), Vol. 2, p. 832.

[12] J. Y. Li, L. Zhang, and S. Ducharme, Appl. Phys. Lett. **90**, 132901 (2007).

[13] A. D. Pomogailo, Russ. Chem. Rev. **71**, 1 (2002).

[14] K. Stoeffler, P. G. Lafleur, and J. Denault, Polym. Eng. Sci. **48**, 1449 (2008).

[15] T. Tanaka, G. C. Montanari, and R. Mulhaupt, IEEE Trans. Dielectr. Electr. Insul. **11**, 763 (2004); T. Tanaka, *ibid.* **12**, 914 (2005).

[16] E. Manias, Nat. Mater. **6**, 9 (2007).

[17] J. G. Zhang, C. A. Wilkie, and E. Manias, J. Nanosci. Nanotechnol. **8**, 1597 (2008).

[18] T. Tanaka, M. Kozako, N. Fuse, and Y. Ohki, IEEE Trans. Dielectr. Electr. Insul. **12**, 669 (2005).

[19] M. Roy, J. K. Nelson, R. K. MacCrone, L. S. Schadler, C. W. Reed, and R. Keefe, IEEE Trans. Dielectr. Electr. Insul. **12**, 629 (2005).

[20] M. C. Costache, M. J. Heidecker, E. Manias, G. Camino, A. Frache, G. Beyer, R. K. Gupta, and C. A. Wilkie, Polymer **48**, 6532 (2007).

[21] E. Manias, J. Zhang, J.-Y. Huh, K. Manokruang, P. Songtipya, and M. M. Jimenez-Gasco, Macromol. Rapid Commun. **30**, 17 (2009).

[22] J. Zhang, E. Manias, G. Polizos, J.-Y. Huh, A. Ophir, P. Songtipya, and M. M. Jimenez-Gasco, J. Adhes. Sci. Technol. **23**, 709 (2009).

[23] C. Zilg, D. Kaempfer, R. Thomann, R. Muelhaupt, and G. C. Montanari, in *IEEE Conference on Electrical and Insulating Dielectric Phenomena (CEIDP 2003)* (IEEE Inc., Piscataway, NJ, 2003), p. 546; R. C. Smith, C. Liang, M. Landry, J. K. Nelson, and L. S. Schadler, IEEE Trans. Dielectr. Electr. Insul. **15**, 187 (2008).

[24] T. J. Lewis, J. Phys. D **23**, 1469 (1990).

[25] L. A. Dissado and J. C. Fothergill, *Electrical Degradation and Breakdown in Polymers* (Peter Peregrinus, London, 1992).

[26] M. A. Lampert and P. Mark, *Current Injection in Solids* (Academic, New York, 1970).

[27] H. Koerner, Y. Luo, X. Li, C. Cohen, R. Hedden, and C. Ober, Macromolecules **36**, 1975 (2003).

[28] Z. Lu, G. Polizos, D. D. Macdonald, and E. Manias, J. Electrochem. Soc. **155**, B163 (2008).

[29] L. Xu, H. Nakajima, E. Manias, and R. Krishnamoorti, Macromolecules **42**, 3795 (2009).

[30] K. Stoeffler, P. G. Lafleur, and J. Denault, Polym. Eng. Sci. **48**, 2459 (2008).

[31] M. Ieda, IEEE Trans. Dielectr. Electr. Insul. **EI-19**, 162 (1984).

[32] V. Kuppa and E. Manias, J. Polym. Sci., Part B: Polym. Phys. **43**, 3460 (2005).

[33] E. Manias and V. Kuppa, Eur. Phys. J. E **8**, 193 (2002).

[34] V. Kuppa, T. M. D. Foley, and E. Manias, Eur. Phys. J. E **12**, 159 (2003).

[35] V. A. Bershtein, and P. N. Yakushev, Adv. Polym. Sci. **230**, 73 (2010).

[36] S. J. Laihonen, U. Gafvert, T. Schutte, and U. W. Gedde, IEEE Trans. Dielectr. Electr. Insul. **14**, 275 (2007).